NJC

ROYAL SOCIETY OF CHEMISTRY

PAPER

View Article Online
View Journal

Cite this: DOI: 10.1039/d3nj04014c

Isonicotinate-Zn(II)/Cd(II) bridged dicobaloximes: synthesis, characterization and electrocatalytic proton reduction studies†

Jitendra Kumar Yadav,[a] Anjali Mishra,[a] Gaurav Kumar Mishra,[b] Sarvesh Kumar Pal,[a] Kedar Umakant Narvekar,[c] Ahibur Rahaman,[d] Nanhai Singh,[a] Prem Lama *[e] and Kamlesh Kumar *[a]

Received 27th August 2023,
Accepted 17th October 2023

DOI: 10.1039/d3nj04014c

rsc.li/njc

Herein, we present the synthesis of two new dicobaloxime complexes, [{ClCo(dmgH)$_2$(4-PyCOO)}$_2$-Zn(DMF)$_2$] (**1**) and [{ClCo(dmgH)$_2$(4-PyCOO)}$_2$Cd(H$_2$O)$_3$(DMF)].4H$_2$O (**2**) bridged by isonicotinate-Zn(II) and Cd(II) moieties. These complexes were synthesized upon reaction of a monomeric chlorocobaloxime [ClCo(dmgH)$_2$(4-PyCOOH)] with Zn(NO$_3$)$_2$·6H$_2$O and Cd(OAc)$_2$·2H$_2$O in a methanol/DMF solvent mixture. Both complexes are fully characterized by UV-Visible, FT-IR, and NMR (^{1}H and ^{13}C{^{1}H}) spectral studies. The solid-state structures are also determined by single-crystal X-ray crystallography. In complex **1**, Zn (II) metal ions reside within a four coordinated distorted tetrahedral geometry (ZnO$_4$) formed by two oxygen atoms of isonicotinate connected to cobaloxime units and two oxygen atoms of DMF molecules. In complex **2**, the Cd(II) metal ion exhibited distorted octahedral geometry (CdO$_6$), with two oxygen atoms of isonicotinate that connect to cobaloxime units, one DMF, and three water molecules. The Co(III) metal center of cobaloxime units in both complexes **1** and **2** displayed distorted octahedral geometry with two dmgH units in the equatorial plane whereas chloride ion (Cl$^-$) and the nitrogen atom of isonicotinate occupy the axial coordination sites. The redox behaviour of both complexes was studied by cyclic voltammetry at variable scan rates in deoxygenated DMF/H$_2$O (95 : 5) solution using 0.1 M TBAPF$_6$ as the supporting electrolyte and a glassy carbon (GC) electrode as the working electrode. Both complexes exhibited similar redox properties and two redox couples Co^{III}/^{II} and Co^{II}/Co^{I} are observed in the reductive scan. Furthermore, complexes are investigated as electrocatalysts for proton reduction in the presence of acetic acid (AcOH) and complex **1** exhibited impressive electrocatalytic activity compared to complex **2** and monomer. The stability study indicated the retention of molecular structural integrity during HER electrocatalytic experiments.

Introduction

The development of renewable energies is receiving great attention in response to the problems associated with the use of non-renewable fossil fuels (coal, oil and natural gas). The conversion of solar energy into storable chemical fuels utilizing photo- and/or electrocatalytic systems is a convincing energy conversion method, which converts water into hydrogen and oxygen.[1–4] Molecular hydrogen is found to be the ultimate clean energy source because of its high energy density (120–142 MJ Kg^{-1}),[5] and also burning of hydrogen produces only water as a waste product. However, the development of efficient catalysts for the widespread production of hydrogen based on non-precious and earth abundant metals is a long-term goal for inorganic chemists. Interestingly, the biological hydrogenases that catalyze the reversible reduction of proton, contain 3d transition metals such as iron and nickel.[6] These biological catalysts operate under weakly acidic aqueous conditions at very low overpotentials with 1000 s^{-1} turnover frequency.[7,8] The active sites of natural hydrogenases inspired the design of earth abundant metal complexes as model compounds of hydrogenases.[9–12]

[a] Department of Chemistry, Institute of Science, Banaras Hindu University Varanasi, Varanasi-221005, India. E-mail: kamlesh.kumar@bhu.ac.in
[b] Department of Chemistry, University of Delhi, Delhi-110007, India
[c] School of Chemical Sciences, Goa University, Taleigao Plateau, Goa-403206, India
[d] Centre for Chemistry and Chemical Engineering, Lund University, Kemicentrum, Solvengatan 39 A, Sweden
[e] CSIR- Indian Institute of Petroleum, Mohkampur, Dehradun-248005, India. E-mail: prem.lama@iip.res.in

† Electronic supplementary information (ESI) available: FT-IR, ^{1}H, and ^{13}C{^{1}H} NMR spectra of complexes, PXRD of complexes, homogeneous electrochemical CV profile, tables of bond angles and bond lengths and details of the weak hydrogen bonding interactions of complex **1** and **2**. CCDC 2233029 and 2233030. For ESI and crystallographic data in CIF or other electronic format see DOI: https://doi.org/10.1039/d3nj04014c

Many of these complexes operate in organic solvents with organic acids as proton sources. In particular, cobaloximes *i.e.* pseudo-octahedral cobalt complexes of glyoximato equatorial ligands and two trans-axial ligands have been extensively studied and showed hydrogen evolution at relatively lower overpotential.[13–20] Initially, cobaloximes were synthesized and studied to mimic the Vitamin B_{12} chemistry,[21–34] but due to their rich coordination chemistry, these have been utilized in many catalytic reactions as well as in organic synthesis.[35–50] In the present time, cobaloxime complexes have been identified as one of the most active series of molecular catalysts for electrocatalytic and photocatalytic hydrogen production because of their low cost, easy synthesis and tuning of catalytic properties by changing the substituents in the equatorial and/or axial ligands.[19,20,37,39,51–59]

It has been shown that the HER catalytic activity of cobaloximes is affected by the substituents at carbon of equatorial dioximes as well as axial pyridine ligands.[28,34,60] The substitution of the electron withdrawing group at dioxime carbon of cobaloxime resulted in the easy reduction of Co(III) to Co(I) but at the same time this makes it weakly nucleophilic toward protonation, hence poor HER activity has been observed.[61] Although the substitution of bridging protons with $-BF_2$ has increased the stability of cobaloximes, it has resulted in poor HER activity.[11] However, using electron donating substituents in the axial pyridine ligand increases the catalytic activity.[62,63] All these results have indicated that varying substituents in the equatorial dioximes as well as axial pyridine ligands affect the HER activity of the cobaloximes. The majority of electro/photocatalytic hydrogen evolution reactions are catalyzed by mononuclear chlorocobaloximes either in solution state or after immobilization on to the surface of solid supports.[56,62–70] Recently, Ott and coworkers have reported cobaloxime based metal organic framework thin films as an electrocatalyst for the hydrogen evolution reaction.[5]

Gupta and co-workers reported the two-dimensional assembly of organocobaloxime with zinc(II) metal ion based paddle wheel center, $Zn_2((OOCR)_4$.[71] This assembly was formed from [MeCo(dmgH)$_2$(4-PyCOOH)], isonicotinic acid and $Zn(NO_3)_2\cdot 6H_2O$ in DMF solvent. Isonicotinic acid is a versatile linker and has been used for the synthesis of a variety of metal–organic frameworks. Using a previous approach as described by Gupta and co-workers,[71] we came up with an idea that chlorocobaloxime containing isonicotinic acid as one axial ligand, [ClCo(dmgH)$_2$(4-PyCOOH)], can be assembled to form a coordination polymer network. However, this resulted in the formation of dicobaloxime assemblies from [ClCo(dmgH)$_2$(4-PyCOOH)] (*vide infra*) with all our tried conditions.

Although the synthesis and characterization of ligand bridged dicobaloximes have been reported in the literature, their applications in electro/photocatalytic hydrogen evolution and oxygen evolution reactions have rarely been reported.[72–74] Therefore, in our continuous effort to understand the HER activity based on new cobaloximes complexes, we report the synthesis and characterization of rare dicobaloxime complexes bridged by isonicotinate-Zn(II)/Cd(II) moieties from mononuclear [ClCo(dmgH)$_2$(4-PyCOOH)]. Complexes are well characterized by combining analytical techniques such as UV-Visible, FT-IR and multinuclear NMR (^{1}H and ^{13}C{^{1}H}) spectral studies. Single crystal X-ray structures have also been determined for both the dicobaloximes. Furthermore the electrochemical properties of both dicobaloximes have been studied by cyclic voltammetry (CV). The CV studies revealed that dicobaloxime complexes exhibited similar redox properties. The spectroscopic and electrochemical studies have indicated that the both cobaloxime units in the dicobaloximes are identical. Furthermore, the electrocatalytic activities of complexes are investigated in the proton reduction to molecular hydrogen under homogeneous conditions using the DMF/H_2O (95 : 5) solvent at the glassy carbon electrode. Dicobaloxime **1** and **2** exhibited electrocatalytic proton reduction activity at two different potentials. Initially a weak HER activity was observed due to Co^{II} cobaloxime species, which was followed by a strong catalytic response for hydrogen evolution possibly associated with Co^{I} species of cobaloxime.

Results and discussion

Synthesis and spectral characterization of dicobaloximes 1 and 2

When the solutions of $Zn(NO_3)_2\cdot 6H_2O$ and $Cd(OAc)_2\cdot 2H_2O$ were independently reacted with mononuclear complex [ClCo(dmgH)$_2$(4-PyCOOH)] in methanol/DMF (80/20, v/v) mixed solvent in a 2 : 1 molar ratio, it resulted in the formation of the heterometallic trinuclear complexes **1** and **2** in good yield (Scheme 1). We also attempted the synthesis of molecular assemblies of [ClCo(dmgH)$_2$(4-PyCOOH)] through coordination with Zn(II) or Cd(II) metal ions with varying ratios of cobaloxime and Zn(II)/Cd(II) metal salts and also in the presence of added isonicotinic acid but in all cases dicobaloxime complexes were isolated as shown in Scheme 1.

The Zn(II) and Cd(II) metal center bridged dicobaloximes (**1** and **2**) are obtained as dark brown solids, which are air and moisture stable. Complexes are insoluble in common organic solvents (dichloromethane, acetone, chloroform and acetonitrile) and sparingly soluble in water and methanol, but soluble in DMSO. Dicobaloxime complexes (**1**, **2**) and monomer [ClCo(dmgH)$_2$(4-PyCOOH)] are fully characterized by UV-Vis, FT-IR, and ^{1}H and ^{13}C{^{1}H} NMR spectral analyses (Fig. 1 and Fig. S1–S10, ESI†). Furthermore, the solid state structures of both complexes have also been confirmed using a single crystal X-ray diffraction (SCXRD) method. Phase purity of the bulk samples of both dicobaloximes **1** and **2** were ascertained by comparing the experimental PXRD patterns with the respective simulated powder patterns obtained from the single crystal data. The peak position of the experimental and the simulated PXRD patterns matched well revealing its phase purity (Fig. S11 and S12, ESI†). The combined spectroscopic studies showed that both cobaloxime units in dicobaloxime complexes are identical. Therefore, the characteristic features of one cobaloxime unit are observed, which has been further corroborated by electrochemical studies (*vide infra*).

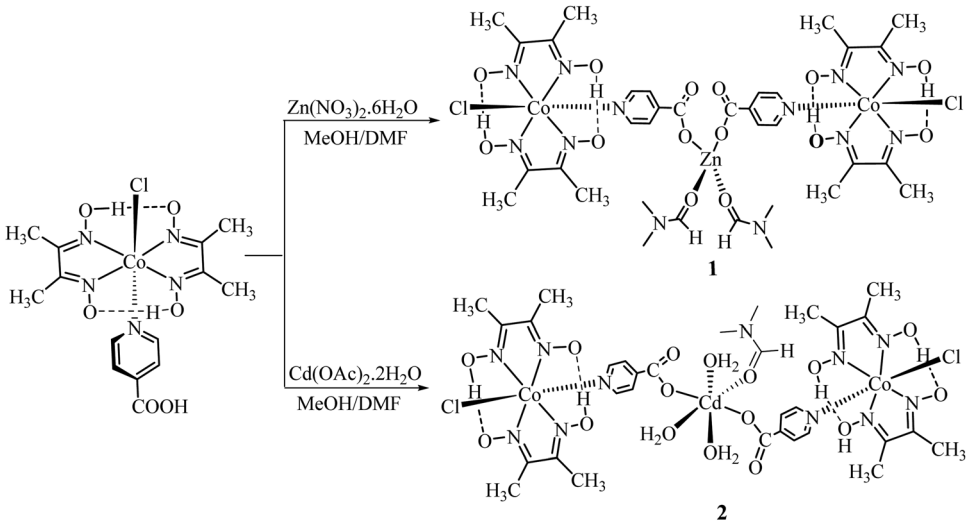

Scheme 1 Synthesis of dicobaloximes (**1** and **2**).

Fourier transform infrared (FT-IR) spectra were recorded and used as a primary characterization technique for the dicobaloximes. The FT-IR spectrum of [Co(dmgH)$_2$(4-PyCOOH)Cl] shows a strong signal at ~1720 cm^{-1} which is attributed to the $\nu_{C=O}$ (Fig. S9, ESI†). However, the IR spectra of complexes **1** and **2** display signals at 1667 and 1651 cm^{-1} respectively for the $\nu_{C=O}$ stretching. The decrease in stretching frequency ($\nu_{C=O}$) of the –COOH functional group of isonicotinic acid indicated the coordination of carboxylate with Zn or Cd metal ions. A similar observation is made toward $\nu_{C=O}$ of DMF where a decrease in the stretching frequency of –CHO ($\nu_{C=O}$) from 1685 cm^{-1} (uncoordinated DMF) to 1643 cm^{-1} (Zn complex) and 1610 cm^{-1} (Cd complex) is observed indicating that the DMF molecule is also coordinated to the Zn and Cd metal ions (Fig. S7 and S8, ESI†).

All UV–Vis absorption spectra were recorded in DMSO solvent in a 10^{-5} molar concentration solution. The UV-Vis absorption spectrum of free isonicotinic acid (Fig. S10, ESI†) shows a strong absorption at 272 nm (0.56×10^5 M^{-1} cm^{-1}) nm attributed to the intraligand π–π* transition[75] whereas monomer chlorocobaloxime [ClCo(dmgH)$_2$(4-PyCOOH)] (Fig. S10, ESI†) shows absorption bands at 260 nm (2.80×10^5 M^{-1} cm^{-1}), 305 nm (0.75×10^5 M^{-1} cm^{-1}), and 375 nm (0.14×10^5 M^{-1} cm^{-1}) due to the intraligand π–π* and metal–ligand centered charge transfer (LMCT) transitions. UV-Vis spectra of dicobaloxime complexes **1** and **2** exhibited very strong absorption bands at ~270 nm (~3.8×10^5 M^{-1} cm^{-1}) and ~305 nm (~1.8×10^5 M^{-1} cm^{-1}), and a weak band at ~370 nm (~0.40×10^5 M^{-1} cm^{-1}) (Fig. 1). The UV-Vis spectral studies indicated that isonictinic acid is coordinated to the cobalt centre. It is also worth noting that the monomer and dicobaloxime complexes have very similar absorption features indicative of identical ligand coordination environments about the metal centres.

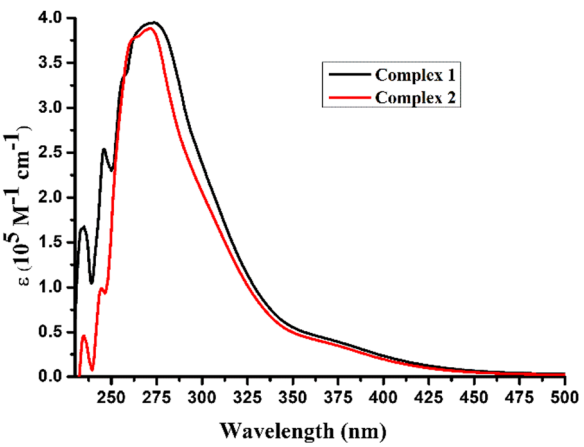

Fig. 1 UV-Vis spectra of dicobaloxime complexes **1** and **2** in DMSO solution at 10^{-5} molar concentration.

Furthermore, the diamagnetic nature of dicobaloximes allowed us to characterize dicobaloxime complexes using multinuclear NMR spectroscopy. ^{1}H and ^{13}C{^{1}H} NMR spectral data for dicobaloximes **1** and **2** are given in the ESI† (Fig. S3–S6). The signals in the ^{1}H NMR spectra of the complexes are easily assigned on the basis of the chemical shifts and their relative intensities. The ^{1}H NMR studies of complexes **1** and **2** revealed that NMR signals of the cobaloxime unit are not greatly affected upon coordination with Zn(II) or Cd(II) metals due to the diamagnetic nature and NMR peaks are consistent with the molecular formulae proposed in Scheme 1. The resonance signals for pyridyl protons (Py$_\alpha$ and Py$_\beta$) of the axial isonicotinate ligand are shifted slightly up-field (~0.1 ppm) in complexes **1** and **2** as compared to mononuclear [ClCo(dmgH)$_2$(4-PyCOOH)] and appeared as two doublets at ~8.10 and ~7.71 ppm in their proton NMR spectra. The resonance signals for O···H–O appeared at ~18.45 ppm whereas dmgH(CH$_3$) protons appeared at ~2.30 ppm in both complexes **1** and **2**. The additional peaks in the proton NMR spectra at chemical shift values of 7.95, 2.89 and 2.73 ppm are attributed to the coordinated DMF molecules. Dicobaloximes are also characterised by ^{13}C{^{1}H} spectral studies where most of the peak positions are similar to the mononuclear cobaloxime except dmgH(CH$_3$) carbon, which showed ~0.3 and ~0.5 ppm

downfield shifts in complexes **1** and **2**, respectively. The resonance signals for methyl groups of coordinated DMF appeared at ~31 and ~35 ppm whereas –CHO carbon appeared at ~167 ppm. The resonance signal for carboxylate carbon of 4-PyCOO was shifted downfield by ~3 ppm and appeared at ~167 and 167.9 ppm in dicobaloximes **1** and **2**, respectively, in comparison to the monomer. We also observed a downfield shift of ~5 ppm in Py_γ carbon of dicobaloximes **1** and **2** compared to monomer chlorocobaloxime.

Single crystal X-ray structures

Single crystals of dicobaloximes **1** and **2**, suitable for X-ray crystallographic studies, were obtained upon slow evaporation of solvent from methanol/DMF solution within 2–3 weeks. Crystallographic data of all crystals and their structure refinement details are presented in Table 1 while the selected bond distances and angles are listed in Tables S2–S5 (ESI†)

Complex **1** crystallises in monoclinic space group *C*2/*c* (Table 1). The asymmetric unit (ASU) consists of one chloro(isonicotinate)cobaloxime unit, half Zn(II) ion and one *N*,*N*′-dimethyl formamide (DMF) molecule. The Zn(II) centre is coordinated in distorted tetrahedral fashion by two oxygen atoms from two different chloro(isonicotinate)cobaloxime units and two DMF molecules in ZnO_4 coordination (Fig. 2). The distance between the zinc ion (Zn1) and carboxylate oxygen atom (O5) is 1.911(1) Å where as in case of the coordinated DMF molecule the distance (O7···Zn1) is found to be 2.008(1) Å. Within the chloro(isonicotinate)cobaloxime unit, the cobalt ion is in a distorted octahedral environment (CoN_5Cl) formed by

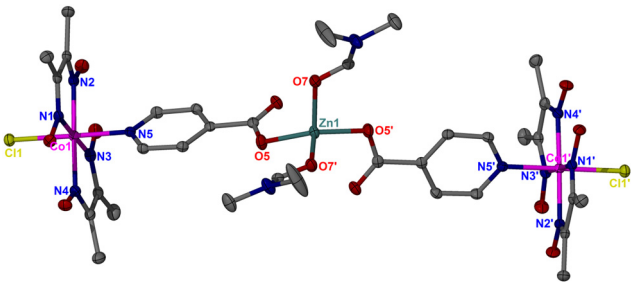

Fig. 2 The molecular structure of complex **1** with ellipsoids at 50% probability showing the atom numbering scheme (hydrogen atoms are omitted for clarity).

the four nitrogen atoms from dimethylglyoxime (Co1···N1 = 1.892(2) Å, Co1···N2 = 1.889(2) Å, Co1···N3 = 1.886(2) Å and Co1···N4 = 1.890(2) Å) in the equatorial plane and axial positions are occupied by one chloride ion (Co1···Cl1 = 2.241(1) Å) and one nitrogen atom from the isonicotinate (Co1···N5 = 1.956(2) Å). The Co–Cl and Co–N bond distances are found to be similar to the precursor complex.[64] The complex does not contain any lattice solvent molecules. Each discrete unit interacts with the neighbouring unit using intermolecular non-classical hydrogen bonding (C–H···O) (Table S1, ESI†). The oxygen atom O2 of the chloro(isonicotinate)cobaloxime unit form the moderate intermolecular hydrogen bonding interaction with the DMF molecule (donor···accepter distances are as follows: C16–H16C···O2 = 3.376(3) Å and C17–H17A···O2 = 3.317(4) Å). The carboxylate oxygen atom (O6) also forms a weak interaction with the DMF molecules from the neighbouring

Table 1 Crystal data and structure refinement parameters for complexes **1** and **2**

Identification code	**1**	**2**
Empirical formula	$C_{34}H_{50}Cl_2Co_2N_{12}O_{14}Zn$	$C_{34}H_{64}Co_2Cl_2N_{12}O_{21}Cd$
Formula weight	1104.99	1278.13
Temperature/K	100(2)	100(2)
Crystal system	monoclinic	monoclinic
Space group	*C*2/*c*	$P2_1/c$
a/Å	20.9563(11)	9.7747(5)
b/Å	19.5207(11)	22.7674(12)
c/Å	11.4806(6)	23.7065(12)
α/°	90	90
β/°	101.314(2)	96.191(2)
γ/°	90	90
Volume/Å^3	4605.2(4)	5245.0(5)
Z	4	4
ρ_{calc}g cm^{-3}	1.594	1.619
μ/mm^{-1}	1.420	1.213
F(000)	2272.0	2624.0
Crystal size/mm^3	0.220 × 0.130 × 0.090	0.127 × 0.056 × 0.052
Radiation	MoKα (*λ* = 0.71073)	MoKα (*λ* = 0.71073)
2Θ range for data collection/°	5.758 to 50	5.138 to 50
Index ranges	$-24 \le h \le 24, -23 \le k \le 23, -13 \le l \le 13$	$-11 \le h \le 11, -27 \le k \le 27, -28 \le l \le 28$
Reflections collected	28 131	59 463
Independent reflections	4043 [R_{int} = 0.0338, R_{Sigma} = 0.0205]	9236 [R_{int} = 0.0632, R_{Sigma} = 0.0423]
Data/restraints/parameters	4043/0/302	9236/40/722
Goodness-of-fit on F^2	1.046	1.049
Final *R* indexes [$I \ge 2\sigma$ (I)]	R_1 = 0.0250, wR_2 = 0.0593	R_1 = 0.0374, wR_2 = 0.0729
Final *R* indexes [all data]	R_1 = 0.0296, wR_2 = 0.0631	R_1 = 0.0537, wR_2 = 0.0793
Largest diff. peak/hole/e Å^{-3}	0.35/−0.38	0.58/−0.42
CCDC Number	2233029	2233030

unit (donor···accepter distance; C16–H16A···O6 = 3.599(3) Å). There are moderate p···π interactions (Fig. S13, ESI†) between the oxygen atoms (O4 and O1) of the cobaloxime unit and centroid (*i*1) of the pyridine ring (O4···*i*1 = 3.223 (1) Å and O1···*i*1 = 3.700(1) Å). In addition, the terminal chloride ion also forms a weak non classical bonding with the methyl group of glyoxime (donor···accepter distance; C1–H1C···Cl1 = 3.758(2) and DMF molecule (C16–H16B···Cl1 = 3.861(3) Å (Fig. S14 and Table S1, ESI†).

Complex **2** crystallises in monoclinic space group $P2_1/c$ (Table 1). The asymmetric unit (ASU) consists of two chloro(isonicotinate)cobaloxime unit, one Cd(II) ion, two *N,N'*-dimethyl formamide (DMF), and seven water molecules (Fig. 3). Both the DMF molecules are disordered where one is coordinated to Cd(II) ion and the other is present in the lattice. Out of seven water molecules present in the ASU, three are coordinated to Cd(II) ion whereas four aqua molecules are present in the lattice. Overall Cd(II) ions form a six coordination mode (CdO_6) with one DMF, three water molecules and two isonicotinate ion that binds the Cd(II) ion in monodentate fashion. It has been revealed from the crystal structure that solvent molecules occupy the four equatorial sites of the octahedral Cd(II) center and both axial sites are occupied by isonicotinate of two cobaloxime units. This arrangement makes the two cobaloxime units identical. The distance between the cadmium ion (Cd1) and carboxylate oxygen atoms (O5 and O11) are found to be 2.323(2) Å and 2.252(3) Å respectively where as in the case of the coordinated DMF molecule the distance (O13···Cd1) is found to be 2.265(3) Å. Within the first chloro(isonicotinate)cobaloxime unit, the Co1 ion is in a distorted octahedral environment (CoN_5Cl) formed by the four nitrogen atoms from dimethylglyoxime (Co1···N1 = 1.899(3) Å, Co1···N2 = 1.895(3) Å, Co1···N3 = 1.900(3) Å and Co1···N4 = 1.894(3) Å), one chloride ion (Co1···Cl1 = 2.237(1) Å) and one nitrogen atom from the isonicotinate (Co1···N5 = 1.956(3) Å). For the second chloro(isonicotinate)cobaloxime unit, the distorted octahedral environment (CoN5O) formed by the four nitrogen atoms from dimethylglyoxime (Co2···N6 = 1.883(3) Å, Co2···N7 = 1.899(3) Å, Co2···N8 = 1.900(3) Å and Co2···N9 = 1.898(3) Å), one chloride ion (Co2···Cl2 = 2.229(1) Å) and one nitrogen atom from the isonicotinate (Co2···N10 = 1.957(3) Å) showed similar coordination bond distances. The lattice water molecules O4W, O5W, O6W and O7WA form non-bonding interactions with the discrete unit (donor···accepter distance; C22–H22C···O4W = 3.337(5) Å, Cl1···O5W = 3.191(3) Å, C5–H5C···O6W = 4.695(5) Å, O7WA–H7WB···O3 = 2.784(4) Å) (Table S1, ESI†). Within O4W and O5W water molecules, there exist strong hydrogen bonding interactions and the donor···acceptor distance between them was found to be 2.771(1) Å. Apart from this, there exist several other strong hydrogen bonding interactions between the lattice water molecules (Table S1, ESI†). The three-dimensional architecture formed by the discrete unit is shown in Fig. S15 and S16 (ESI†).

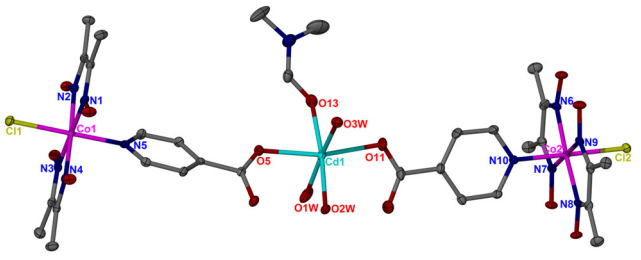

Fig. 3 Diagram showing the binding of the cobaloxime unit and Cd(II) centre with 50% probability ellipsoids (disordered fraction of coordinated DMF, lattice solvent molecules and hydrogen atoms are omitted for clarity).

Electrochemical properties of dicobaloximes (1 and 2)

The electrochemical properties of dicobaloximes **1** and **2** were studied by cyclic voltammetry (CV) and compared with those of its monomer [ClCo(dmgH)$_2$(4-PyCOOH)] to determine the reduction potentials that further relate the electrocatalytic proton reduction activity (*vide infra*). The two reduction events are observed in each case (Fig. 4a). The CV of **1** shows a reversible redox wave at $E_{1/2}$ *ca.* = −1.00 V (scan rate = 0.1 V s^{-1}), which is assigned to the $Co^{II/I}$ couple. The reductive feature associated with the $Co^{III/II}$ redox couple is observed as a quasi-reversible redox wave at −0.58 V. The CV responses of Cd(II) bridged dicobaloxime **2** is similar to that of Zn(II) bridged dicobaloxime **1** and exhibited a reversible redox wave at $E_{1/2}$ *ca.* −0.88 V (scan rate = 0.1 V s^{-1}), which is assigned to the $Co^{II/I}$ couple. The reductive features associated with the $Co^{III/II}$ redox couple are poorly defined in this case and observed as an irreversible wave at *ca.* −0.42 V.[57] It is observed that the potential of the $Co^{II/I}$ couple is shifted cathodically by ∼190 mV and ∼70 mV in complexes **1** and **2**, respectively, relative to that of the $Co^{II/I}$ couple observed in the mononuclear form ([ClCo(dmgH)$_2$(4-PyCOOH)]). A relatively more cathodic shift in the reduction potentials for $Co^{II/I}$ was observed as compared to $Co^{III/II}$ in complexes **1** and **2** and with respect to the monomer indicating an increase in electron density on the Co(II) center with the coordination of isonicotinate to Zn(II) and Cd(II) ions in respective complexes. It is also interesting to note that complex **1** exhibits a quasi-reversible $Co^{III/II}$ redox peak compared to irreversible $Co^{III/II}$ in complex **2** and monomer (Fig. 4a).

The electrochemical studies of dicobaloximes indicated that both cobaloxime units are identical and hence electrochemical redox responses associated with one cobalt center are observed. The peaks currents of complexes **1** and **2** are higher relative to the monomer because of the redox activity by two Co centers. Furthermore, Zn(II) and Cd(II) metal ions are redox inactive but these metal ions affect the electronic properties of the cobalt center upon coordination with cobaloxime units and formation of dicobaloxime. The $Co^{II/I}$ redox couple in complex **1** exhibits enhanced reversible and additionally quasi-reversibility in $Co^{III/II}$ compared to complex **2** and monomer. Therefore, this may cause complex **1** to exhibit the enhanced electrocatalytic activity. Furthermore, the scan rate variation did not show any significant change in the redox properties in the negative potential window for these complexes (Fig. S17a and c, ESI†).

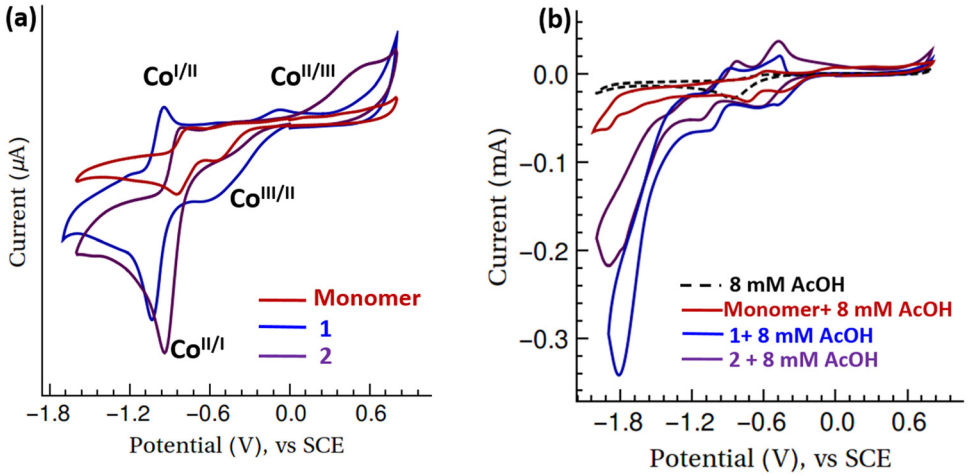

Fig. 4 Cyclic voltammograms recorded in DMF: water (95/5, v/v) containing 0.1 M [NBu_4][PF_6] as the supporting electrolyte at 0.1 V s^{-1} containing (a) 1 mM of monomer [ClCo(dmgH)$_2$(4-PyCOOH)] (red trace), complex **1** (blue trace), and complex **2** (purple trace), and (b) 1 mM complexes in the presence of 8 mM acetic acid and the dotted black CV is recorded in 8 mM acetic acid.

The peak current varies linearly with the square root of the scan rate and follows the Randles–Sevcik equation. This confirms the diffusion-controlled electron transfer behaviour. The diffusion coefficients were determined from the slope (see Fig. S17b and d, ESI†) of peak current (i_p) *versus* square root of scan rate ($\nu^{1/2}$) using Randles–Sevcik eqn (1), given as

$$i_p = 0.4463nFA[\mathrm{Co(III)}]\left(\frac{nF\nu D_{cat}}{RT}\right)^{1/2} \quad (1)$$

where, i_p = peak current, n = 1 (number of electrons transferred), A = 0.07 cm^2 (working electrode area), F = 96 500 C $mole^{-1}$ (Faraday constant), R = 8.314 J K^{-1} $mole^{-1}$ (gas constant), T = 298 K (temperature), D_{cat} = diffusion coefficient of catalyst, and ν = scan rate (V s^{-1}). The diffusion coefficients for complexes **1** and **2** were obtained as 3.40 × 10^{-6} and 3.03 × 10^{-5} cm s^{-1}, respectively. The characteristic redox potentials and diffusion coefficients are listed in Table 2.

After the electrochemical characterization and redox behaviour studies of dicobaloximes, we investigated the electrocatalytic ability of these complexes for the reduction of proton to the dihydrogen in the presence of acetic acid (AcOH) as a proton source. We recorded the CV of complexes **1**, **2** and monomer in the presence of 8 mM AcOH (Fig. 4b). It is interesting to note that complex **1** exhibits an enhanced electrocatalytic performance for hydrogen production as compared to complex **2** and monomer. The magnitude of the onset potential for proton reduction follows the order as **1** (−1.26 V)< **2** (−1.41 V) < monomer (−1.61 V). Furthermore, we have extensively analysed complexes **1** and **2** by varying the acid and complex concentration in the subsequent sections.

Electro-catalytic proton reduction to dihydrogen

The results of electrocatalytic studies with varying AcOH concentrations are displayed in Fig. 5. The main features are: (i) the current of the catalytic peak remains unchanged upon the addition of more than 50 mM of AcOH for Complex **1** with i_c/i_p = 72 and 20 mM of AcOH for complex **2** with i_c/i_p = 16 (Fig. 5c and Fig. S18a, b, ESI†), suggesting that complex **1** is a more efficient electrocatalyst as compared to complex **2**, (ii) the strong catalytic wave appears for complex **1** at a catalytic half-wave potential ($E_{cat/2}$) of −1.58 V, whereas the relatively weaker catalytic wave appears for complex **2** at $E_{cat/2}$ of −1.63 V upon the addition of 8 mM AcOH (see Fig. 5a and b), (iii) the main electrocatalytic event occurs at the more negative potential with respect to the reduction potential for complex **1** (−1.04 V) and **2** (−0.94 V) for $Co^{II/I}$ (Table 2) showing that the active catalytic species contains a reduced Co(I) intermediate that results in the formation of Co(III)–H intermediate in the presence of AcOH. The weak catalytic waves at less negative potentials are associated with Co(II) cobaloxime species formed upon substitution of Cl^- with a solvent molecule and continuous presence of Co^{II} species in the reaction solution. The initial weak catalytic wave followed by a strong catalytic hydrogen evolution wave at $E_{cat/2}$ of −1.58 V (complex **1**) and −1.63 V (complex **2**) are attributed to the one electron reduction of Co^{III}–H to a highly basic Co^{II}–H intermediate species, which undergoes protonation to produce the molecular hydrogen and generate the Co^{II} catalyst. The high electron density on Co^{II} in complex **1** as compared to **2** and monomer results in the facile protonation of Co^{II} and yield of Co^{III}–H. The observed mechanistic trend is in coherence with earlier studies for various cobaloximes[56,62,76] and cobalt metal based complexes.[77–79] The characteristic peaks and onset potentials for the HER are listed in Table 3.

Table 2 Comparison of redox properties for Co^{II}/Co^{I} of 1 mM of complexes **1**, **2** and monomer containing 0.1 M $TBAPF_6$ in DMF/H_2O (95/5, v/v) at a scan rate of 100 mV s^{-1}

Complex	E_{pc}/V (Co^{II}/Co^{I})	E_{pa}/V (Co^{I}/Co^{II})	ΔE_p/V	E^0/V	D_{cat} (cm^2 s^{-1})
1	−1.04	−0.96	0.08	−1.00	3.40 × 10^{-6}
2	−0.94	−0.83	0.11	−0.88	3.03 × 10^{-5}
Monomer	−0.85	−0.77	0.08	−0.81	—

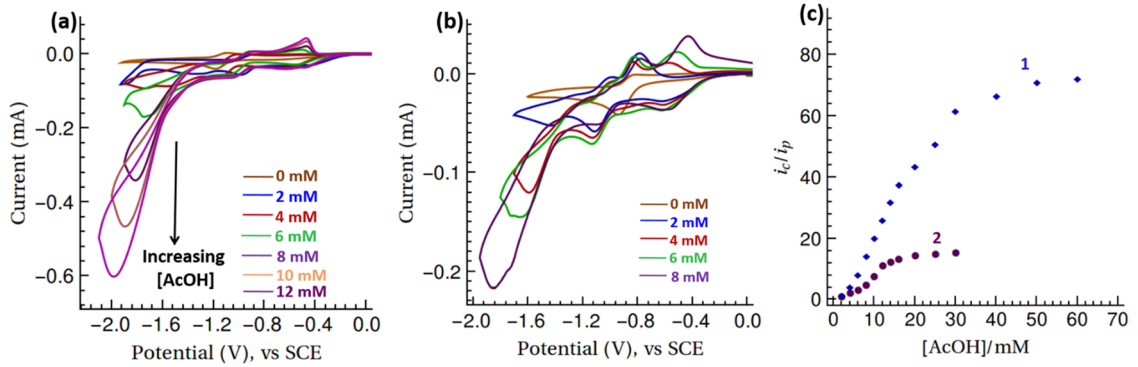

Fig. 5 Variation of the catalytic peak current of 1 mM complexes (a) **1**, and (b) **2** with increasing concentration of acetic acid. (c) Dependence of relative catalytic peak current (i_c/i_p) on the increasing concentration of acetic acid in 1 mM of complexes **1** and **2**. 0.1 M $TBAPF_6$ is used as a supporting electrolyte and CVs are recorded at 0.1 V s^{-1} scan rate.

Fig. 5c shows that the catalytic peak current (i_c) increases with increasing concentration of AcOH. The i_c/i_p *versus* varying AcOH concentration in DMF/H_2O solution with 1 mM of complexes **1** and **2** at 0.1 V s^{-1} shows linear dependence in the low AcOH concentration regime and therefore follows the second order catalytic rate on acid concentration. However, in the high AcOH concentration limit, the catalytic peak current becomes independent of AcOH and therefore, the proton reduction follows the zero-order kinetics.[56,80] Also, the catalytic current increases with increasing concentrations of complex **1** in 8 mM AcOH concentration (Fig. S19a, ESI†). The plot of i_c *versus* various concentrations of complex exhibits the linear dependency that indicates the first-order catalytic rate with respect to catalyst concentration (Fig. S19b, ESI†). The mathematical formulation of catalytic current depending on the acid and catalyst concentrations following a catalytic reaction (second-order in acid and first-order in catalyst concentration) is given by[81]

$$i_c = nFA[\mathrm{Co(III)}]\sqrt{Dk_{obs}[H^+]^2} \quad (2)$$

where n is the number of electrons transferred (2 for the reduction of proton to dihydrogen) and k_{obs} is the rate constant of the reaction. In the high AcOH concentration limit in Fig. 5c, the i_c/i_p becomes acid independent therefore the rate constant (k_{obs}) or the turnover frequency (TOF) are estimated using the following eqn (3)[82,83] as

$$\frac{i_c}{i_p} = \frac{n}{0.4463}\sqrt{\frac{RTk_{obs}}{F\nu}} \quad (3)$$

The k_{obs} is estimated from the acid independent i_c/i_p value for complexes **1** and **2**. The estimated k_{obs} values and other characteristic potentials are listed in Table 3.

Table 3 Electrochemical properties of 1 mM of complexes **1**, **2**, and monomer in DMF/H_2O (95/5, v/v) with 0.1 M $TBAPF_6$ and 8 mM AcOH at a 0.1 V s^{-1} scan rate

Complex	E^{onset}/V	$E_{cat/2}$/V	i_c/i_p	k_{obs}/s^{-1}
1	−1.26	−1.58	72	1006
2	−1.41	−1.63	16	49
Monomer	−1.61	−1.86	—	—

Proposed mechanism

Based on the electrochemical experimental analysis and consideration of previously reported mechanisms for Co^{III} chloro complexes,[56,62,77,78] the plausible mechanism is proposed in Fig. 6. The electrochemical CV experiment in Fig. 5 suggests that initially, the Co^{III} complex was reduced to Co^{II} species following the one-electron reduction process. Furthermore, the dissociation of the chloro ligand results in the formation of five-coordinate Co^{II} species which undergoes subsequent one-electron reduction to yield a highly nucleophilic Co^{I} as a reactive intermediate. The Co^{I} species is quickly protonated and generates the Co^{III}–H intermediate.[76] Co^{III}–H is further reduced to a highly basic Co^{II}–H intermediate which undergoes protonation to generate H_2. The protonation of Co^{II}–H to generate H_2 has been considered a rate limiting step.[84] This

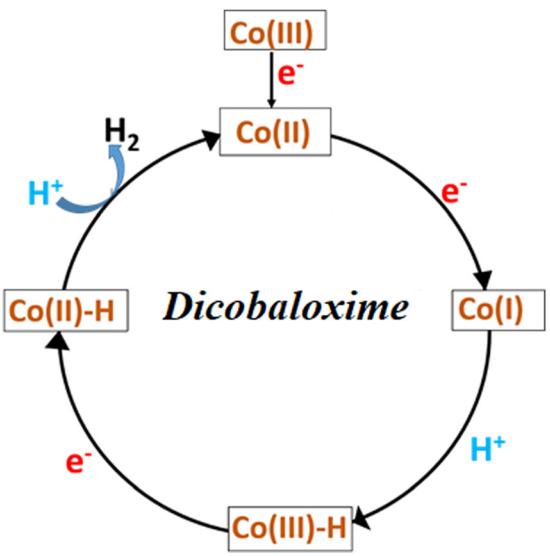

Fig. 6 Plausible mechanism of the hydrogen evolution reaction by dicobaloxime bridged by isonicotinate-Zn(II)/Cd(II).

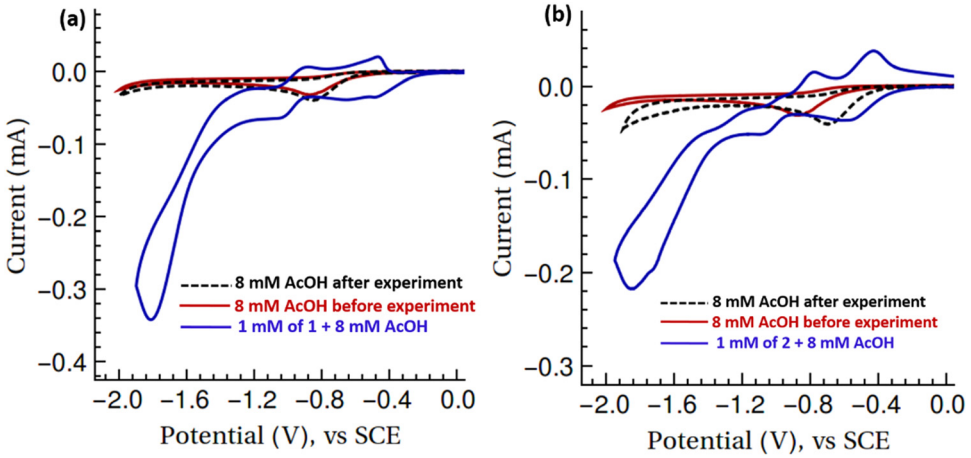

Fig. 7 The dashed black trace corresponds to 8 mM AcOH solution before the catalytic experiment, the solid red trace is after the catalysis experiment, and the blue trace corresponds to CV in 8 mM AcOH solution at a 100 mV s^{-1} scan rate.

suggests that the catalytic activity can be regulated by enhancing the basicity of this species *via* introducing the electron donating substituents to the cobaloxime.

Stability of complexes

Complexes **1** and **2** were highly stable in the absence and presence of 25 mM acetic acid as time dependent UV-Vis spectroscopy measurement confirms no substantial spectral changes over a period of 24 h (Fig. S20, ESI†). Additionally, the rinse experiment was performed, which confirms no significant current difference in CV (Fig. 7) which was recorded in the presence of 8 mM AcOH in DMF/H_2O containing 0.1 M TBAPF6 at 0.1 V s^{-1} before and after the experiment for both complexes **1** and **2**. This confirms the molecular electrocatalyst driven HER process in the solution rather than the working electrode surface modified with the deposition of nanoparticulated materials during the electrocatalytic experiments. This also suggested that the molecular integrity of these catalysts is maintained during electrocatalysis.

Conclusions

The present work describes the synthesis and characterization of two new dicobaloxime complexes bridged by Zn(II) and Cd(II) metal ions. The single crystal X-ray structures of dicobaloximes revealed the distorted tetrahedral and octahedral geometries around Zn(II) and Cd(II) metal ions, respectively. The geometry around the cobalt center in the cobaloxime unit is distorted octahedral with two dioximes ligands occupying the equatorial plane and axial coordination is occupied by chloride and nitrogen of isonicotinate ligands. The combined spectroscopic and electrochemical studies indicated that two cobaloxime units are identical and therefore, the characteristic features of only one cobaloxime unit are observed. Electrochemical studies showed $Co^{III/II}$ at a less negative potential and the $Co^{II/I}$ redox couple at higher negative potentials. Furthermore, dicobaloximes are active catalysts for the electrochemical proton reduction to dihydrogen in DMF/H_2O solution. Initially, weak HER waves are observed at less negative potentials associated with Co^{II} cobaloxime species and a strong catalytic HER event is observed at a more negative potential which is attributed to the Co^{I} cobaloxime centric HER process. The stability studies of dicobalximes *via* rinse experiments show the molecular integrity of complexes maintained during electrocatalytic proton reduction.

Experimental section

General methods and materials

All reactions were carried out in the open and at room temperature unless specifically mentioned. Solvents were purified using standard procedures and dried before use according to the requirements.[85] All of the commercially available reagents of analytical grade were purchased from Sigma-Aldrich, Spectrochem, S. D. Fine Chemicals, or Avra and were used as received without further purification. Melting points of the complexes were determined in open capillaries with a Gallenkamp apparatus and are uncorrected. FT-IR spectra in the 4000–400 cm^{-1} region were recorded as KBr disks using a PerkinElmer FT-IR spectrophotometer. ^{1}H and $^{13}C\{^{1}H\}$ NMR spectra were obtained in DMSO-d_6 on a JEOL ECZ500 MHz FT NMR spectrometer. Tetramethylsilane (TMS) was used as an internal standard for recording the NMR spectra. UV-visible absorption spectra in solution (DMSO) state were obtained on a Shimadzu UV-1800 instrument.

Single crystal X-ray diffraction (SCXRD)

Both the single crystal data were collected on a Bruker APEX-III D8 Quest diffractometer fitted with an Oxford 700Plus cryostat Cryosystems and MoKα monochromator radiation (λ = 0.71073 Å) using an Incoatec IμS microsource. Data integration was performed using standard procedures and the SAINT[86] package. The absorption corrections and other systematic error corrections were performed using SADABS.[87,88] The structures were solved

by SHELXT and refined using SHELXL-2019.[89] X-Seed[90] was employed as the graphical interface for the SHELX program suite. Hydrogen atoms were placed in calculated positions using riding models for complexes **1** and **2**.

The DMF molecules in complex **2** are severely disordered which are modelled successfully. The coordinated DMF molecule is disordered into two fractions (0.8 and 0.2) whereas the lattice DMF molecule is disordered over three positions (0.65, 0.2 and 0.15 fractions). Only the major fractions are refined anisotropically in the case of DMF. Out of seven water molecules, one lattice water molecule (O7W) is disordered over two fractions (O7WA and O7WB) where the lower fraction with 0.2 occupancy (OW7B) is refined isotropically. The rest of the water molecules are refined anisotropically. The hydrogen atoms for all water molecules were located using the riding model. For water molecules, non-bonding interactions are calculated with the major fraction as well as non-disordered lattice water molecules.

Electrochemistry

Cyclic voltammetry experiments were carried out in deoxygenated DMF/H_2O (95/5, V/V) solutions with 0.1 M $TBAPF_6$ as the supporting electrolyte. The working electrode (glassy carbon of 3 mm diameter) was polished with 0.3 μm alumina slurry followed by washing with ethanol and distilled water prior to electrochemical measurements. The counter electrode was a platinum wire and a standard Calomel electrode was employed as the reference electrode. All potentials were referenced to the SCE. A Metrohm Autolab M204 potentiostat was used for all electrochemical measurements. Studies of electrocatalytic proton reduction were carried out by adding AcOH (Sigma-Aldrich).

Synthesis of [ClCo(dmgH)$_2$(4-PyCOOH)]

The complex was synthesized following the procedure reported in the literature.[60] $CoCl_2{\cdot}6H_2O$ (1.0 g, 4.2 mmol), dimethylglyoxime (1.10 g, 9.5 mmol) and NaOH (0.17 g, 4.2 mmol) were dissolved in 95% ethanol (20 mL) and heated to 70 °C. Isonicotinic acid (0.517g, 4.2 mmol) was then added and the resulting solution was cooled to the room temperature. This was followed by the passing of a stream of air through the solution for 1 h, which resulted in the precipitation of a brown solid. The solid precipitate was filtered and successively washed with water (5 mL), ethanol (2 ×5 mL) and diethyl ether (3 × 5 mL). The product was obtained as a brown solid which was used for further reaction without purification. Yield: 1.350 g (∼70%). Mp: 210 °C. FT-IR (KBr, cm^{-1}): 3449 (ν_{O-H}), 2925 (ν_{C-H}), 1720 ($\nu_{C=O}$, carboxylate), 1560 ($\nu_{C=N}$, dmgH), 1235 (ν_{N-O}). ^{1}H NMR (500 MHz, DMSO-d_6): δ 18.42 (s, 2H, OHO), 8.21 (d, J = 5 Hz, 2H), 7.85 (d, J = 5 Hz, 2H), 2.31 (s, 12H). $^{13}C\{^1H\}$ NMR (125 MHz, DMSO-d_6): 164.28, 152.41, 151.05, 141.05, 124.82, 12.35. UV-Vis: DMSO, λ_{max} (nm), ε (M^{-1} cm^{-1}): 260 (2.80×10^5), 305 (0.75×10^5), 375 (0.14×10^5).

Synthesis of [{ClCo(dmgH)$_2$(4-PyCOO)}$_2$Zn(DMF)$_2$] (1)

[ClCo(dmgH)$_2$(4-PyCOOH)] (100 mg, 0.223 mmol) was dissolved in a 10 mL solvent mixture of MeOH and DMF (8 : 2 v/v) and $Zn(NO_3)_2{\cdot}6H_2O$ (33 mg, 0.111 mmol) was added to the solution. The reaction mixture was stirred for three hours at room temperature followed by filtration to remove any solid and the filtrate was kept aside for crystallization. Needle shaped dark brown coloured crystals of complex **1** were obtained in 2–3 weeks. Yield: 40 mg (∼33%). Mp: 200–204 °C. FT-IR (KBr, cm^{-1}): ν = 3439 (ν_{O-H}), 3068 (ν_{C-H}), 1667 ($\nu_{C=O}$, carboxylate), 1643 ($\nu_{C=O}$, DMF), 1563 ($\nu_{C=N}$, dmgH), ν = 1242 (ν_{N-O}). ^{1}H NMR (500 MHz, DMSO-d_6): 18.45 (s, 4H, OHO), 8.10 (d, J = 5 Hz, 4H), 7.95 (s, 2H, DMF-CHO), 7.72 (d, J = 5 Hz, 4H), 2.89 (s, 6H), 2.73 (s, 6H), 2.30 (s, 24H). $^{13}C\{^1H\}$ NMR (125 MHz, DMSO-d_6): δ 167.09, 162.57, 152.81, 150.88, 145.61, 125.42, 35.97, 30.94, 12.77. UV-Vis: DMSO, λ_{max} (nm), ε (M^{-1} cm^{-1}): 271 (3.95×10^5), 309 (1.84×10^5), 371 (0.42×10^5).

Synthesis of [{ClCo(dmgH)$_2$(4-PyCOO)}$_2$Cd(H$_2$O)$_3$(DMF)].4H$_2$O (2)

[ClCo(dmgH)$_2$(4-PyCOOH)] (100 mg, 0.223 mmol) was dissolved in 10 mL solvent mixture of MeOH and DMF (8 : 2 v/v) and $Cd(OAc)_2{\cdot}2H_2O$ (30 mg, 0.111 mmol) was added to the solution. The reaction mixture was stirred for three hours at room temperature followed by filtration to remove any solid and filtrate was kept aside for crystallization. Needle shaped dark brown coloured crystals of complex **2** were obtained in 2–3 weeks. Yield: 48 mg (∼38%). Mp: 250–253 °C. FT-IR (KBr, cm^{-1}): 3436 (ν_{O-H}), 2925 and 2852 (ν_{C-H}), 1651 ($\nu_{C=O}$, carboxylate), 1610 ($\nu_{C=O}$, DMF), 1551 ($\nu_{C=N}$, dmgH), 1237 (ν_{N-O}). ^{1}H NMR (500 MHz, DMSO-d_6): 18.46 (s, 4H, OHO), 8.09 (d, J = 5 Hz, 4H), 7.95 (s, 1H, DMF-CHO) 7.72 (d, J = 10 Hz, 4H), 2.89 (s, 3H), 2.73 (s, 3H), 2.31 (s, 24H). $^{13}C\{^1H\}$ NMR (125 MHz, DMSO-d_6): δ 167.93, 162.49, 152.70, 150.73, 147.10, 125.82, 35.96, 31.21, 12.80. UV-vis: DMSO, λ_{max} (nm), ε (M^{-1} cm^{-1}): 271 (3.87×10^5), 304 (1.84×10^5), 370 (0.37×10^5).

Author contributions

The manuscript was written through contribution of all authors.

Conflicts of interest

There are no conflicts of interest to declare.

Acknowledgements

We gratefully acknowledge financial support from the University Grants Commission (UGC), New Delhi, for the award of UGC-BSR Research Start-Up-Grant (No. F. 30-431/2018 (BSR)), and the Banaras Hindu University–Seed Grant under the IoE Scheme. Jitendra Kumar Yadav and Anjali Mishra acknowledge CSIR, INDIA, for the senior research fellowship and Sarvesh Kumar Pal thanks UGC, INDIA, for SRF. Prem Lama gratefully acknowledges financial support from the Department of Science and Technology (DST), New Delhi, in the form of a DST-INSPIRE Faculty award [DST/INSPIRE/04/2017/000249].

References

1 M. G. Walter, E. L. Warren, J. R. McKone, S. W. Boettcher, Q. Mi, E. A. Santori and N. S. Lewis, *Chem. Rev.*, 2010, **110**, 6446–6473.
2 S. Ardo, D. Fernandez Rivas, M. A. Modestino, V. Schulze Greiving, F. F. Abdi, E. Alarcon Llado, V. Artero, K. Ayers, C. Battaglia, J.-P. Becker, D. Bederak, A. Berger, F. Buda, E. Chinello, B. Dam, V. Di Palma, T. Edvinsson, K. Fujii, H. Gardeniers, H. Geerlings, S. M. H. Hashemi, S. Haussener, F. Houle, J. Huskens, B. D. James, K. Konrad, A. Kudo, P. P. Kunturu, D. Lohse, B. Mei, E. L. Miller, G. F. Moore, J. Muller, K. L. Orchard, T. E. Rosser, F. H. Saadi, J.-W. Schüttauf, B. Seger, S. W. Sheehan, W. A. Smith, J. Spurgeon, M. H. Tang, R. van de Krol, P. C. K. Vesborg and P. Westerik, *Energy Environ. Sci.*, 2018, **11**, 2768–2783.
3 D. Gust, T. A. Moore and A. L. Moore, *Acc. Chem. Res.*, 2009, **42**, 1890–1898.
4 H. B. Gray, *Nat. Chem.*, 2009, **1**, 112.
5 S. Roy, Z. Huang, A. Bhunia, A. Castner, A. K. Gupta, X. Zou and S. Ott, *J. Am. Chem. Soc.*, 2019, **141**, 15942–15950.
6 W. Lubitz, H. Ogata, O. Rudiger and E. Reijerse, *Chem. Rev.*, 2014, **114**, 4081–4148.
7 A. K. Jones, E. Sillery, S. P. Albracht and F. A. Armstrong, *Chem. Commun.*, 2002, 866–867.
8 C. Madden, M. D. Vaughn, I. Díez-Pérez, K. A. Brown, P. W. King, D. Gust, A. L. Moore and T. A. Moore, *J. Am. Chem. Soc.*, 2012, **134**, 1577–1582.
9 X. Chu, J. Jin, B. Ming, M. Pang, X. Yu, C.-H. Tung and W. Wang, *Chem. Sci.*, 2019, **10**, 761–767.
10 A. G. Maher, G. Passard, D. K. Dogutan, R. L. Halbach, B. L. Anderson, C. J. Gagliardi, M. Taniguchi, J. S. Lindsey and D. G. Nocera, *ACS Catal.*, 2017, **7**, 3597–3606.
11 X. Hu, B. S. Brunschwig and J. C. Peters, *J. Am. Chem. Soc.*, 2007, **129**, 8988–8998.
12 V. Artero and M. Fontecave, *Coord. Chem. Rev.*, 2005, **249**, 1518–1535.
13 Y. Chen, H. Chen and H. Tian, *Chem. Commun.*, 2015, **51**, 11508–11511.
14 B. Reuillard, J. Warnan, J. J. Leung, D. W. Wakerley and E. Reisner, *Angew. Chem., Int. Ed.*, 2016, **128**, 4020–4025.
15 E. S. Andreiadis, P.-A. Jacques, P. D. Tran, A. Leyris, M. Chavarot-Kerlidou, B. Jousselme, M. Matheron, J. Pécaut, S. Palacin and M. Fontecave, *Nat. Chem.*, 2013, **5**, 48–53.
16 P. Zhang, M. Wang, C. Li, X. Li, J. Dong and L. Sun, *Chem. Commun.*, 2010, **46**, 8806–8808.
17 G.-G. Luo, K. Fang, J.-H. Wu, J.-C. Dai and Q.-H. Zhao, *Phys. Chem. Chem. Phys.*, 2014, **16**, 23884–23894.
18 B. J. Fisher and R. Eisenberg, *J. Am. Chem. Soc.*, 1980, **102**, 7361–7363.
19 P.-A. Jacques, V. Artero, J. Pécaut and M. Fontecave, *Proc. Natl. Acad. Sci. U. S. A.*, 2009, **106**, 20627–20632.
20 N. Kaeffer, M. Chavarot-Kerlidou and V. Artero, *Acc. Chem. Res.*, 2015, **48**, 1286–1295.
21 G. N. Schrauzer and J. Kohnle, *Chem. Ber.*, 1964, **97**, 3056–3064.
22 G. N. Schrauzer, G. Parshall and E. Wonchoba, *Inorg. Synth.*, 1968, **11**, 61–70.
23 G. Schrauzer, *Angew. Chem. Int. Ed.*, 1976, **15**, 417–426.
24 R. Banerjee, *Chemistry and Biochemistry of B12*, John Wiley & Sons, 1999.
25 K. L. Brown, *Chem. Rev.*, 2005, **105**, 2075–2150.
26 B. van Arkel, J. van der Baan, S. Balt, M. de Bolster, R. van Delft, G. Klumpp, H. De Koning and Y. van den Winkel, *Rec. Trav. Chim. Pays Bas*, 1988, **107**, 23–24.
27 L. Randaccio, N. B. Pahor, E. Zangrando and L. Marzilli, *Chem. Soc. Rev.*, 1989, **18**, 225–250.
28 K. Kumar and B. D. Gupta, *J. Organomet. Chem.*, 2011, **696**, 3785–3791.
29 K. Kumar and B. D. Gupta, *J. Organomet. Chem.*, 2011, **696**, 3343–3350.
30 K. Kumar and B. D. Gupta, *J. Organomet. Chem.*, 2011, **696**, 2280–2286.
31 B. D. Gupta and K. Kumar, *Inorg. Chim. Acta*, 2011, **372**, 8–16.
32 K. Kumar and B. D. Gupta, *J. Organomet. Chem.*, 2010, **695**, 2233–2239.
33 K. Kumar, S. Kumar and B. D. Gupta, *J. Organomet. Chem.*, 2010, **695**, 512–517.
34 G. Dutta, K. Kumar and B. Gupta, *Organometallics*, 2009, **28**, 3485–3491.
35 X. Sun, J. Chen and T. Ritter, *Nat. Chem.*, 2018, **10**, 1229–1233.
36 H. Cao, H. Jiang, H. Feng, J. M. C. Kwan, X. Liu and J. Wu, *J. Am. Chem. Soc.*, 2018, **140**, 16360–16367.
37 K. E. Dalle, J. Warnan, J. J. Leung, B. Reuillard, I. S. Karmel and E. Reisner, *Chem. Rev.*, 2019, **119**, 2752–2875.
38 K. C. Cartwright and J. A. Tunge, *ACS Catal.*, 2018, **8**, 11801–11806.
39 K. C. Cartwright, A. M. Davies and J. A. Tunge, *Eur. J. Org. Chem.*, 2020, 1245–1258.
40 W.-Q. Liu, T. Lei, S. Zhou, X.-L. Yang, J. Li, B. Chen, J. Sivaguru, C.-H. Tung and L.-Z. Wu, *J. Am. Chem. Soc.*, 2019, **141**, 13941–13947.
41 S. Hou, H. Yang, B. Cheng, H. Zhai and Y. Li, *Chem. Commun.*, 2017, **53**, 6926–6929.
42 Z. Liu, Y. Wang, K. Liu, S. Wang, H. Liao, Y. Zhu, B. Hou, C. Tan and G. Liu, *Front. Chem.*, 2021, 781.
43 A. Kilic, M. Ulusoy, E. Aytar and M. Durgun, *J. Ind. Eng. Chem.*, 2015, **24**, 98–106.
44 J. Li, C.-Y. Huang, J.-T. Han and C.-J. Li, *ACS Catal.*, 2021, **11**, 14148–14158.
45 M. Kojima and S. Matsunaga, *Trends Chem.*, 2020, **2**, 410–426.
46 H. Zhao, A. J. McMillan, T. Constantin, R. C. Mykura, F. Julia and D. Leonori, *J. Am. Chem. Soc.*, 2021, **143**, 14806–14813.
47 M. Tada and K. Kaneko, *J. Org. Chem.*, 1995, **60**, 6635–6636.
48 M. Tada and Y. Hanaoka, *J. Organomet. Chem.*, 2000, **616**, 89–95.

49 R. R. Pidaparthi, M. E. Welker and C. S. Day, *Organometallics*, 2006, **25**, 974–981.
50 M. W. Wright, T. L. Smalley Jr, M. E. Welker and A. L. Rheingold, *J. Am. Chem. Soc.*, 1994, **116**, 6777–6791.
51 D. Aand, S. Sk, K. Kumar, U. Pal and A. K. Singh, *Int. J. Hydrogen Energy*, 2022, **47**, 7180–7188.
52 D. Dolui and A. Dutta, *Chem. Commun.*, 2020, **56**, 14841–14844.
53 S. Roy, A. Bhunia, N. Schuth, M. Haumann and S. Ott, Sustain, *Energy Fuels*, 2018, **2**, 1148–1152.
54 M. Cai, F. Zhang, C. Zhang, C. Lu, Y. He, Y. Qu, H. Tian, X. Feng and X. Zhuang, *J. Mater. Chem. A*, 2018, **6**, 138–144.
55 T. Banerjee, F. Haase, G. K. Savasci, K. Gottschling, C. Ochsenfeld and B. V. Lotsch, *J. Am. Chem. Soc.*, 2017, **139**, 16228–16234.
56 J. L. Dempsey, B. S. Brunschwig, J. R. Winkler and H. B. Gray, *Acc. Chem. Res.*, 2009, **42**, 1995–2004.
57 F. Lakadamyali and E. Reisner, *Chem. Commun.*, 2011, **47**, 1695–1697.
58 J. Willkomm, N. M. Muresan and E. Reisner, *Chem. Sci.*, 2015, **6**, 2727–2736.
59 D. Dolui, S. Khandelwal, A. Shaik, D. Gaat, V. Thiruvenkatam and A. Dutta, *ACS Catal.*, 2019, **9**, 10115–10125.
60 A. Panagiotopoulos, K. Ladomenou, D. Sun, V. Artero and A. G. Coutsolelos, *Dalton Trans.*, 2016, **45**, 6732–6738.
61 V. Artero, M. Chavarot-Kerlidou and M. Fontecave, *Angew. Chem. Int. Ed. Engl.*, 2011, **50**, 7238–7266.
62 D. W. Wakerley and E. Reisner, *Phys. Chem. Chem. Phys.*, 2014, **16**, 5739–5746.
63 M. Razavet, V. Artero and M. Fontecave, *Inorg. Chem.*, 2005, **44**, 4786–4795.
64 X.-W. Song, H.-M. Wen, C.-B. Ma, H.-H. Cui, H. Chen and C.-N. Chen, *RSC Adv.*, 2014, **4**, 18853–18861.
65 F. Wen, J. Yang, X. Zong, B. Ma, D. Wang and C. Li, *J. Catal.*, 2011, **281**, 318–324.
66 Y. Xu, R. Chen, Z. Li, A. Li, H. Han and C. Li, *ACS Appl. Mater. Interfaces*, 2017, **9**, 23230–23237.
67 S. Troppmann and B. König, *Chem. – Eur. J.*, 2014, **20**, 14570–14574.
68 F. Lakadamyali, A. Reynal, M. Kato, J. R. Durrant and E. Reisner, *Chem. – Eur. J.*, 2012, **18**, 15464–15475.
69 B. Reuillard, J. Warnan, J. J. Leung, D. W. Wakerley and E. Reisner, *Angew. Chem., Int. Ed.*, 2016, **55**, 3952–3957.
70 I. K. Sideri, G. Charalambidis, A. G. Coutsolelos, R. Arenal and N. Tagmatarchis, *Nanomaterials*, 2022, **12**, 3077.
71 S. Kumar and B. D. Gupta, *Inorg. Chem.*, 2011, **50**, 9207–9209.
72 D. Mandal and B. D. Gupta, *Eur. J. Inorg. Chem.*, 2006, 4086–4095.
73 X.-F. Liu, Y.-X. Zhang and J. Yan, *Trans. Met. Chem.*, 2015, **40**, 305–311.
74 C. N. Valdez, J. L. Dempsey, B. S. Brunschwig, J. R. Winkler and H. B. Gray, *Proc. Natl. Acad. Sci. U. S. A.*, 2012, **109**, 15589–15593.
75 W.-T. Chen, *J. Chem. Crystallogr.*, 2021, **51**, 116–123.
76 J. L. Dempsey, J. R. Winkler and H. B. Gray, *J. Am. Chem. Soc.*, 2010, **132**, 16774–16776.
77 E. S. Wiedner and R. M. Bullock, *J. Am. Chem. Soc.*, 2016, **138**, 8309–8318.
78 Z. Wang, Y. Liu, T. Li, Y.-Z. He, E.-C. Han, Y.-L. Chen, X.-Y. Jiang, C.-L. Ni, L.-M. Yang and W. Liu, *Electrocatalysis*, 2023, **14**, 752–762.
79 N. Queyriaux, D. Sun, J. Fize, J. Pécaut, M. J. Field, M. Chavarot-Kerlidou and V. Artero, *J. Am. Chem. Soc.*, 2020, **142**, 274–282.
80 A. Z. Haddad, S. P. Cronin, M. S. Mashuta, R. M. Buchanan and C. A. Grapperhaus, *Inorg. Chem.*, 2017, **56**, 11254–11265.
81 A. D. Wilson, R. H. Newell, M. J. McNevin, J. T. Muckerman, M. R. DuBois and D. L. DuBois, *J. Am. Chem. Soc.*, 2006, **128**, 358.
82 A. M. Appel, D. L. DuBois and M. Rakowski DuBois, *J. Am. Chem. Soc.*, 2005, **127**, 12717.
83 L. Gan, T. L. Groy, P. Tarakeshwar, S. K. Mazinani, J. Shearer, V. Mujica and A. K. Jones, *J. Am. Chem. Soc.*, 2015, **137**, 1109–1115.
84 J. L. Dempsey, J. R. Winkler and H. B. Gray, *J. Am. Chem. Soc.*, 2010, **132**, 1060–1065.
85 B. S. Furniss, *Vogel's textbook of practical organic chemistry*, Pearson Education, India, 1989.
86 N. SAINT, Inc.: Madison, WI, 2003.
87 S. G. SADABS, *Bruker AXS Inc*.: Madison, WI, 2002.
88 R. H. Blessing, *Acta Crystallogr., Sect. A: Found. Crystallogr.*, 1995, **51**, 33–38.
89 G. Sheldrick, *Acta Crystallogr., Sect. A: Found. Crystallogr.*, 2008, **64**, 112–122.
90 L. J. Barbour, *J. Appl. Crystallogr.*, 2020, **53**, 1141–1146.